Advanced Persistent Scatterer Interferometry products

Michele Crosetto[1], Maria C. Ramlie[1], Anna Barra[1], María Cuevas-González[1], Riccardo Palamà[1], Oriol Monserrat[1], Qi Gao[1], Saeedeh Shahbazi[1]

[1] Centre Tecnològic de Telecomunicacions de Catalunya - CERCA (CTTC-CERCA), Castelldefels, Barcelona, Spain
(mcrosetto, mramlie, abarra, mcuevas, rpalama, omonserrat, qgao, sshahbazi)@cttc.cat

Keywords: SAR, interferometry, deformation, advanced products, added-value products.

Abstract

The Persistent Scatterer Interferometry technique has undergone strong development in the last decades. Despite this, there is still a need to improve its products. This paper describes a set of advanced Persistent Scatterer Interferometry products. The first product is the result of a joint processing of SAR data coming from multiple sensors. In this paper, we present a multi-sensor framework that integrates data coming from the C-band Sentinel-1 and X-band TerraSAR-X sensors. The second class of products are derived starting from the standard results of Persistent Scatterer Interferometry. Such products address specific application needs and that offer higher-level data with respect to the classical products. They include the so-called Active Deformation Area maps, the Classified Active Deformation maps, and the Building Differential Deformation maps that are focused on the spatial gradient of deformations. All these products are easy-to-handle, also for GIS non-experts. They can facilitate the interpretation and exploitation of the Persistent Scatterer Interferometry results for different types of applications.

1. Introduction

Persistent Scatterer Interferometry (PSI) is a consolidated active remote sensing technique to measure and monitor land deformation (Crosetto et al., 2016). The technique has experienced an intense development in the last 25 years. In the academic field, this technique and its parent technique, i.e. interferometric SAR, have generated a conspicuous amount of journal papers, being several times published in the top-ranked journals worldwide. In the business sector, there are nowadays dozens of companies that provide commercial services based on PSI. At institutional level, several initiatives have promoted PSI-based ground deformation services that cover entire countries or, in the case of the European Ground Motion Service (EGMS), most of the European continent (Crosetto et al., 2020; Crosetto and Solari, 2023).

In this paper we describe some advanced PSI products. The first one involves the processing of SAR data coming from multiple sensors. The PSI technique is usually based on the exploitation of data coming from the same SAR sensor, or SAR sensors with identical characteristics, e.g. Sentinel-1A and Sentinel-1B (Crosetto et al., 2016). In the approach outlined in the next section, we present a multi-sensor PSI framework that integrates C-band Sentinel-1 and X-band TerraSAR-X data.

The second class of advanced products includes those that are derived starting from the results of PSI. The outcome of any PSI processing is a cloud of geocoded measurement points that contain the estimated deformation time series over the observation period, with one estimated deformation in correspondence to each acquisition date of the used SAR stack. If the analysed area is wide, the corresponding point clouds, which are usually stored as CVS files, can be huge. This is for instance the case of the points clouds coming from EGMS, which are delivered by bursts of the original Sentinel-1 images. CSV file sizes vary depending on the number of measurement points contained in each EGMS product. The size ranges from a few tens of Mb, up to more than 3 Gb. The bigger files usually correspond to urban areas, where the measurement point density is the highest. Visualizing large CSV files using standard tools like can be a problem. Moreover, it is important to note that visualizing large CSV files directly in a GIS environment, e.g. using QGIS, can be very slow if not impossible. In these cases, the potential users experience barriers in the analysis of such huge point clouds. This represents a clear limit for PSI exploitation and user uptake.

Considering these aspects, in this paper we present a set of products that address specific application needs and that offer higher-level products with respect to the standard PSI products. These products are easy-to-handle also for GIS non-experts. This can facilitate the interpretation and exploitation of the PSI results for different types of applications.

2. Multi-sensor InSAR approach

As already mentioned above, the standard PSI techniques exploit interferometric SAR data coming from sensors with identical characteristics. In the frame of the SMILE project, we are developing a multi-sensor PSI framework that integrates SAR data coming from different sensors.

The use of multiple sensors for deformation monitoring offers in principle two interesting advantages. First, it increases the temporal sampling, and hence the capability to describe temporally the evolution of deformation. This allows us to reduce the risk of phase unwrapping, which in case of Sentinel-1 occurs with deformation above the limit of 2 mm/day. Note that this limit affects pairs of measurement points, i.e. it is a differential limit that does not apply to absolute values. The second advantage is the increase in the number of observations, which confers redundancy and robustness on the estimation process.

The approach has been tested using C-band Sentinel-1 and X-band TerraSAR-X data. It combines the dense temporal coverage of Sentinel-1 with the high spatial resolution of TerraSAR-X, allowing deformation signals to be captured more robustly than with either sensor alone. The complete multi-sensor PSI chain has not been finalized yet. As an example, Figure 1 shows an example of intermediate PSI product, the residual topographic error, estimated using Sentinel-1 and TerraSAR-X data over a mining area.

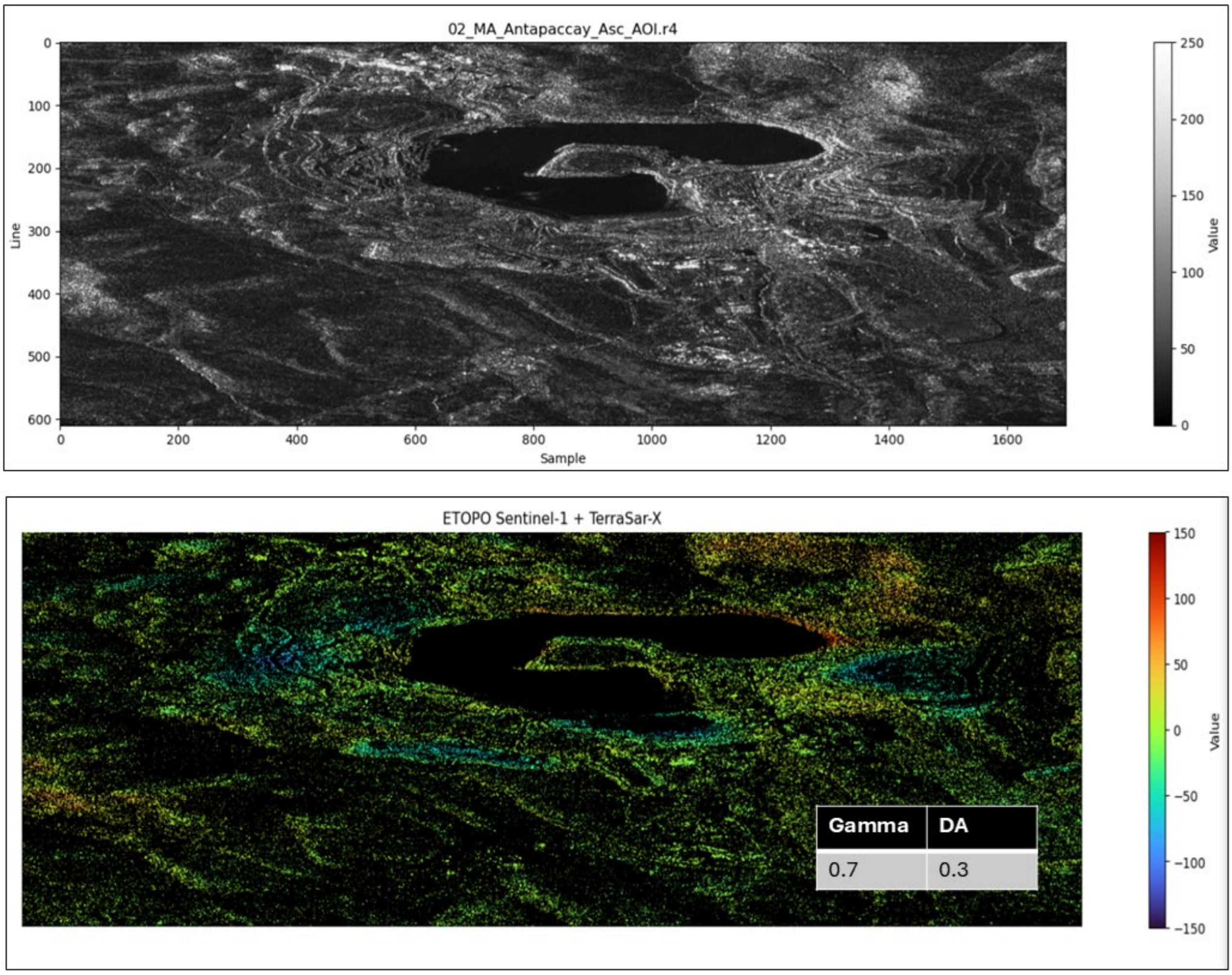

Figure 1: Example of PSI intermediate result coming from Sentinel-1 and TerraSAR-X data. Mean amplitude of the area of interest (above). Residual topographic error estimated using jointly the two SAR datasets (below).

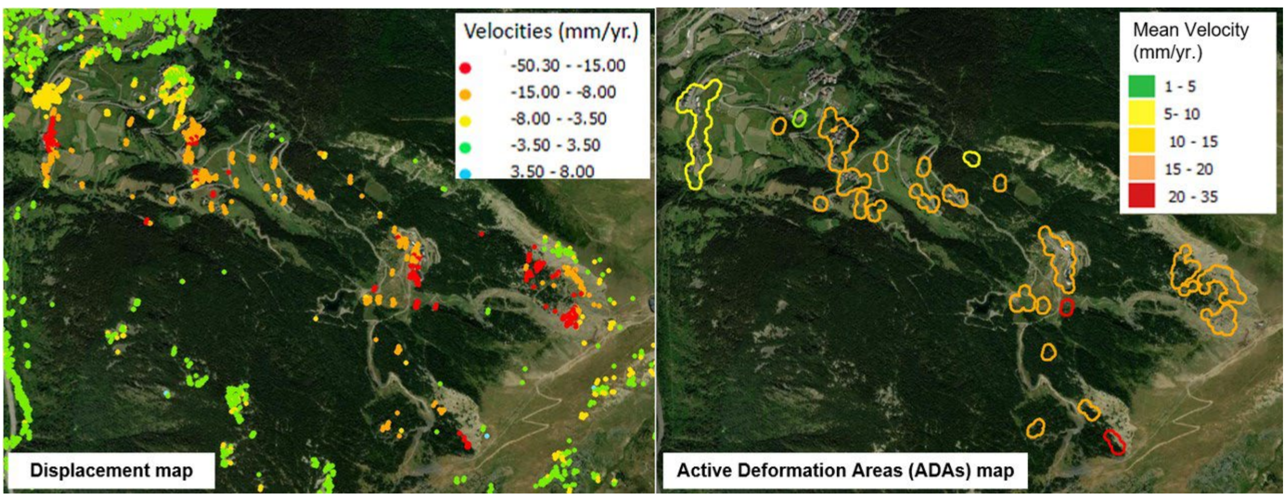

Figure 2: Example of ADA map over a landslide area. Colour-coded deformation velocity map superposed to an orthoimage of the area of interest (left). Set of polygons representing the ADA of the same area (right). The ADAs are colour-coded according to their mean velocity.

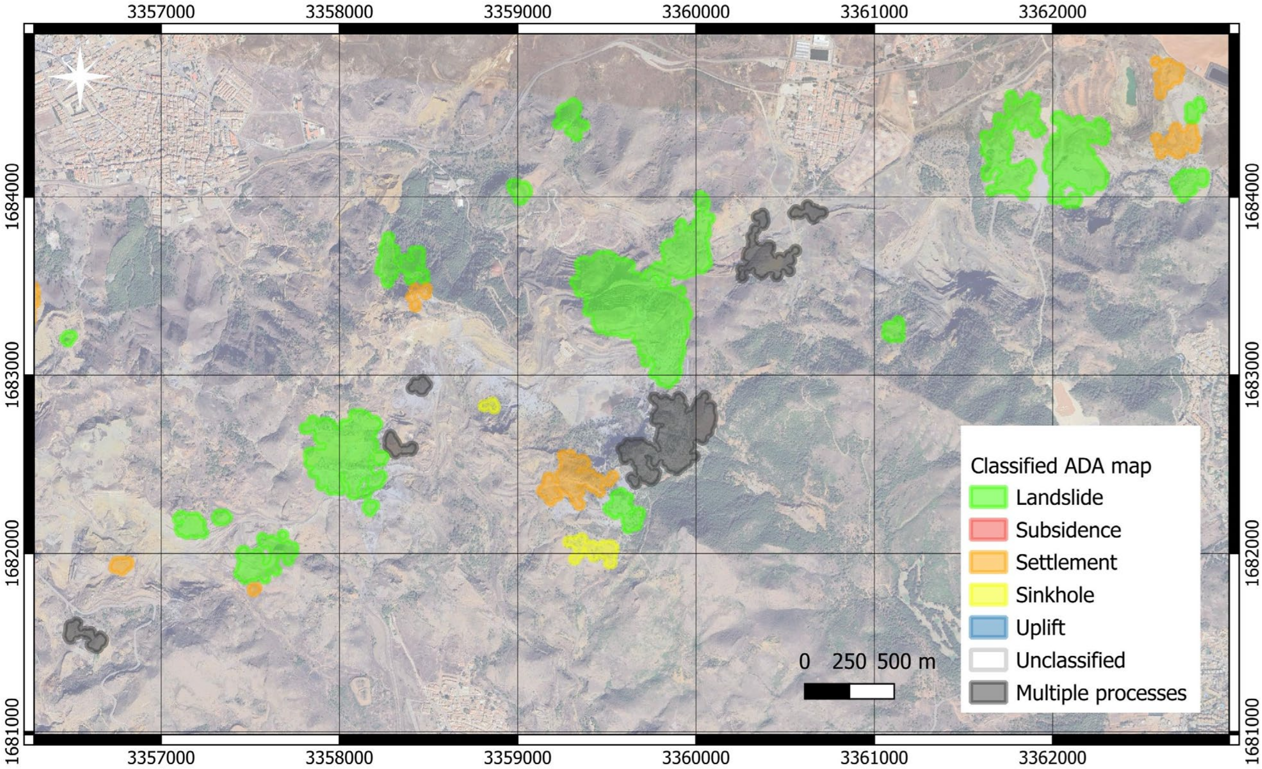

Figure 3: Example of classified ADA map. Colour-coded polygons representing the ADAs of the area of interest. The example includes landslides, settlements, sinkholes, and deformation due to multiple processes.

3. Active Deformation Area maps

The Active Deformation Area (ADA) product is an example of easy-to-handle and high-level PSI product. As mentioned above, the PSI product can contain millions of measurement points. The goal is to facilitate the data handling, interpretation and exploitation, especially for non-expert users. The key idea here is to focus the attention only on the active measurement points, i.e. those that have a given level of deformation. For this purpose, a threshold on the deformation velocity is applied.

The ADA maps are generated from PSI point clouds using a data clustering procedure that filters and drastically reduces the volume of the original PSI datasets. The original approach is described in Barra et al. (2017). The measurement points clusters (ADAs) are groups of neighbouring measurement points that have deformation velocities above a given threshold. A minimum number of close points is required. Each ADA is assigned a quality index, which accounts for the noise of the deformation time series and the spatial homogeneity of the clustered measurement point deformations. An example of ADA map is shown in Figure 2.

The use of the ADAs is now rather widespread. A Europe-wide map (European ADA web map), derived from EGMS Basic data, can be found at http://groundmotionADAs.com.

4. Classified ADA maps

A natural evolution of the ADA maps involves enriching the attributes of the ADA clusters. In Navarro et al. (2020), this is achieved using an automated classification procedure that identifies the specific geological or anthropogenic drivers behind observed deformations. By utilizing a decision tree supported by external data, such as Digital Terrain Models (DTM), geological maps, and various inventories, each ADA is assigned a thematic label, distinguishing between phenomena like subsidence, uplift, landslides, sinkholes, etc. An example of classified ADA map is shown in Figure 3.

More advanced classification frameworks have been investigated. Using machine learning, Palamà et al. (2024) introduce a supervised classifier based on the Extreme Gradient Boosting (XGBoost) technique. This approach was successfully applied to process massive EGMS datasets covering all of Italy. A further contribution by Rivera-Rivera et al. (2024) makes use of machine learning as an essential tool for the rapid interpretation of large-scale PSI data.

The most recent advancement in this field shifts the focus from the nature of the movement to its consequences through the creation of the so-called ADA impact maps. As described by Mileu et al. (2025), this product is specifically designed for decision-makers to evaluate the potential risk associated with detected deformations. The impact is estimated by calculating the relationship between the magnitude of the process and the exposure of the affected area. While magnitude is determined by factors such as surface area, deformation velocity, and time-series behaviour, exposure accounts for the population, buildings, and critical infrastructure, such as roads and railways, that fall within the ADA boundaries.

This approach categorizes potential impact into low, medium, and high classes. Because these maps are only derived from remote sensing data, they provide a comprehensive overview of structural and geological risks that can be generated entirely without physical access to the site. This makes the ADA impact map a key tool for infrastructure management.

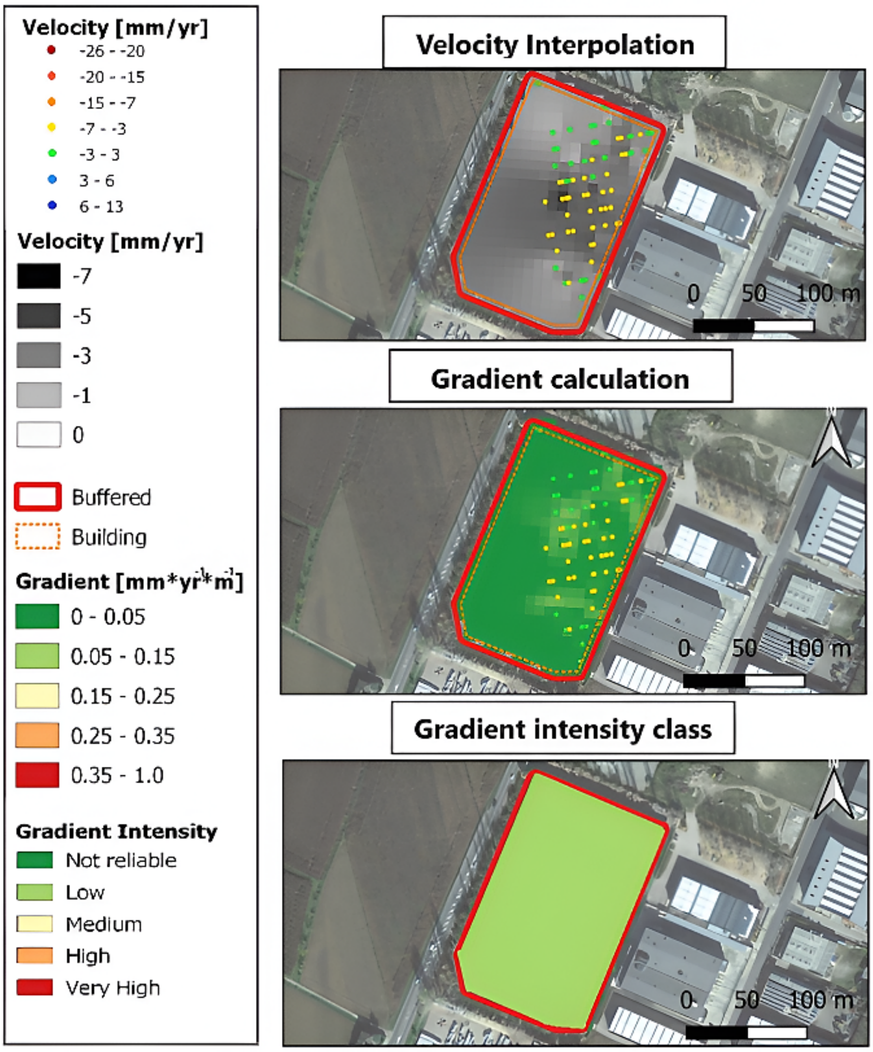

Figure 4: Deformation gradient classification starting from the deformation velocity points coming from the EGMS Basic product.

5. Building differential deformation (BDD) maps

Another example of advanced PSI product is represented by the map of spatial differential deformations (Shahbazi et al., 2024; 2025). Here the focus is on the spatial gradient of deformation, which is a geometric parameter that can be directly related to damages of buildings, structures and infrastructures.

The procedure, which is named Building Differential Deformation (BDD), requires in input a PSI point cloud and a vector map of elements of interest of the analysed area, namely buildings, structures and infrastructures. For all elements that are sampled by enough measurement points, the procedure estimates the spatial gradient of the deformation, retaining for each element the maximum local gradient. The maximum gradient values are then classified in classes of potential damage (Shahbazi et al., 2024).

Figure 4 shows the estimation of the deformation gradient class of a building, starting from the EGMS velocity values. The first step is the interpolation of the deformation velocity. The second one involves calculating the spatial gradient. Finally, the third step involves the classifications of the gradients. The reliability of the procedure depends on the number of measurement points falling inside a given element.

6. Derived products from BDD

The BDD map can be used as main input for generating further added-value products. For this purpose, we use additional information. The first one is the displacement velocity. Then building construction age is included, based on the assumption that older buildings with higher displacement velocities are more vulnerable to damage than newer ones. Finally, population data are also integrated to consider the number of affected people.

Figure 5 shows the three matrixes used for integrating the BDD with the displacement velocity, the building construction age, and exposed population. For each additional layer of information, a separate map is generated. In the first step, we incorporate the displacement velocity into the BDD map. The output is the so-called "Ground Deformation Intensity" map.

Secondly, we assume that the building construction year can influence the probability of experiencing structural damage. This is clearly a simplification, because structural vulnerability is also influenced other factors such as construction materials, building reinforcement, design standards, and building usage. These additional factors are not considered in the current implementation of the analysis due to the unavailability of reliable data. By incorporating the building age, we generate the so-called “Potential Damage Intensity” map.

In the third step, we focus on the number of people who are potentially affected by building damage. By incorporating population data into the analysis, we generate the so-called “Potential Impact” map, which represents the main output of the procedure.

The “Potential Impact” map contains four classes, with class 1 indicating minimal impact and class 4 signifying severe impact. The “Potential Impact” map is useful to identify areas that need prioritized attention and resources for effective risk mitigation. An example of “Potential Impact” map is shown in Figure 6, which concerns the city of Torremolinos (Spain). It is worth underlining that this map only contains the buildings that have enough measurement points.

a

Ground Deformation Intensity				
Velocity (mm/yr) \ Gradient	G < 0.05	0.05 < G < 0.12	0.12 < G < 0.20	G > 0.20
Abs (vel) < 3	1	2	3	4
3 <Abs (vel) <16	2	3	3	4
Abs (vel) > 16	2	3	4	4

b

Potential Damage Intensity			
Ground Deformation Intensity \ Construction year	2022-2000	2000-1960	1960 > year
1_Very Low	1	1	2
2_ Low	1	2	3
3_Medium	2	3	4
4_ High	3	4	4

c

Potential Impact			
Potential Damage Intensity \ Population	0-10	10-100	100 > population
1_Very Low	1	1	2
2_ Low	1	2	3
3_Medium	2	3	4
4_ High	3	4	4

Very low
Low
Medium
High

Figure 5: Matrixes used in the analysis: (a) Fusion of velocity and gradient values; (b) Introduction of the year of construction; (c) Introduction of the population data.

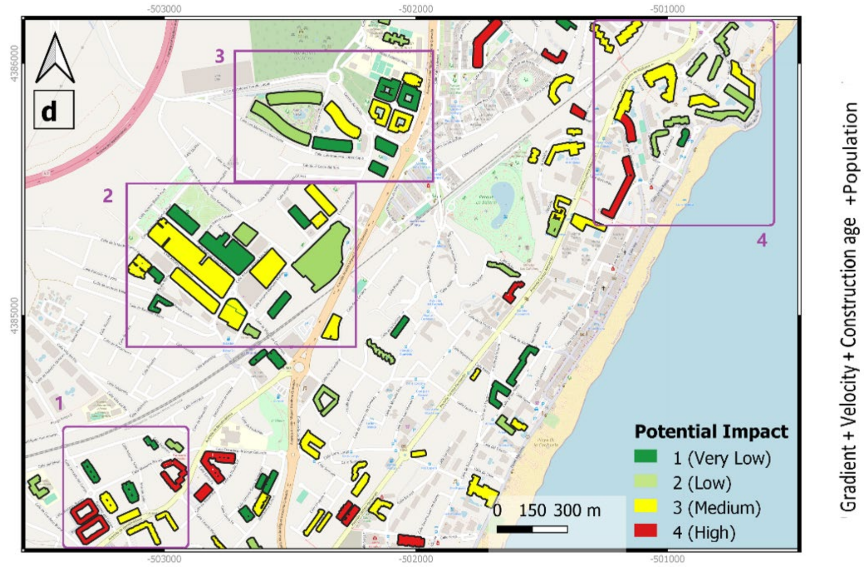

Figure 6: Example of “Potential Impact” map that covers the city of Torremolinos (southern Spain).

7. Conclusions

PSI products are widely used in the academic field, in the business sector, and at institutional level, e.g. see the Copernicus service called European Ground Motion Service.

In this paper we have described some advanced PSI products. The first one involves the processing of SAR data coming from multiple sensors. We are currently working on a framework that integrates C-band Sentinel-1 and X-band TerraSAR-X data.

We have then presented a set of products that are derived from the PSI results. Such products are easy-to-handle, especially for GIS non-experts. The following products have been proposed:

- Active Deformation Area (ADA) maps.
- Classified ADA maps.
- Building Differential Deformation (BDD) maps.
- Derived products from BDD.

These products facilitate the interpretation and exploitation of the PSI results for different types of applications.

Acknowledgements

The authors acknowledge funding from the European Union’s Horizon Europe Research and Innovation Programme through the Doctoral Network of the Marie Sklodowska-Curie Actions SMILE, under grant agreement No. 101073281.

References

Barra, A., Solari, L., Béjar-Pizarro, M., Monserrat, O., Bianchini, S., Herrera, G., et al. (2017). A methodology to detect and update active deformation areas based on Sentinel-1 SAR images. *Remote sensing*, 9(10), 1002.

Crosetto, M., Monserrat, O., Cuevas-González, M., Devanthéry, N., Crippa, B. (2016). Persistent Scatterer Interferometry: A review, *ISPRS Journal of Photogrammetry and Remote Sensing* 115, pp. 78-89, https://doi.org/10.1016/j.isprsjprs.2015.10.011.

Crosetto, M., Solari, L., Mróz, M., Balasis-Levinsen, J., Casagli, N., Frei, M., Oyen,, A., Moldestad, D.A., Bateson, L., Guerrieri, L., Comerci, V., Andersen, H.S. (2020) The evolution of wide-area DInSAR: From regional and national services to the European Ground Motion Service. *Remote Sensing* 12(12), 2043.

Crosetto, M., Solari, L. (2023). *Satellite Interferometry Data Interpretation and Exploitation: Case Studies from the European Ground Motion Service (EGMS)*. Elsevier.

Mileu, N., Barra, A., Ezquerro, P., Oliveira, S.C., Garcia, R.A., Melo, R., ..., Zêzere, J.L. (2025). ADAImpact Tool: Toward a European Ground Motion Impact Map. *ISPRS International Journal of Geo-Information*, *14*(10), 389.

Navarro, J.A., Tomás, R., Barra, A., Pagán, J.I., Reyes-Carmona, C., Solari, L., Vinielles, J.L., Falco, S., Crosetto, M. (2020). ADAtools: Automatic detection and classification of Active Deformation Areas from PSI displacement maps. *Int. Journal of Geo-Information*, 9, 584.

Palamà, R., Barra, A., Cuevas-González, M., Monserrat, O., Crosetto, M. (2024). Ground motion classification from European Ground Motion Service data using Extreme Gradient Boosting. IGARSS 2024.

Rivera-Rivera, J.S., Béjar Pizarro, M., Aguilera Alonso, H., Ezquerro, P., Guardiola-Albert, C., Monserrat, O. (2024). Automated classification of ground deformation processes in Spain: a machine learning approach using a novel national InSAR-based database. In EGU General Assembly Conference Abstracts, EGU24-8369.

Shahbazi, S., Barra, A., Gao, Q., Crosetto, M. (2024). Detection of buildings with potential damage using differential deformation maps. *ISPRS Journal of Photogrammetry and Remote Sensing*, *218*, 57-69.

Shahbazi, S., Barra, A., Navarro, J.A., Crosetto, M. (2025). From EGMS to Potential Damage Maps: Assessing the Potential Impact of Ground Motion on Exposed Buildings. *IEEE Journal of Selected Topics in Applied Earth Observations and Remote Sensing*.